

Supplementary Information - Electrical Breakdown of Suspended Mono- and Few-Layer Tungsten Disulfide via Sulfur Depletion Identified by *in-Situ* Atomic Imaging

Ye Fan^{1†}, Alex W. Robertson^{1,2*†}, Yingqiu Zhou¹, Qu Chen,¹ Xiaowei Zhang³, Nigel D. Browning^{2,4},
Haimei Zheng³, Mark H. Rümmeli^{5,6}, Jamie H. Warner^{1*}

¹Department of Materials, University of Oxford, Parks Road, Oxford, OX1 3PH, United Kingdom

²Physical & Computational Science Directorate, Pacific Northwest National Laboratory, Richland,
WA 99352 United States

³Materials Sciences Division, Lawrence Berkeley National Laboratory, Berkeley, California 94720,
United States

⁴Department of Materials Science and Engineering, University of Washington, Seattle, WA 98195,
United States

⁵Soochow Institute for Energy and Materials Innovations, College of Physics, Optoelectronics and
Energy, Collaborative Innovation Center of Suzhou Nano Science and Technology, Key Laboratory
of Advanced Carbon Materials and Wearable Energy Technologies of Jiangsu Province, Soochow
University, Suzhou 215006, China

⁶Centre of Polymer and Carbon Materials, Polish Academy of Sciences, M. Curie-Sklodowskiej 34,
Zabrze 41-819, Poland

*alex.w.robertson@gmail.com; jamie.warner@materials.ox.ac.uk

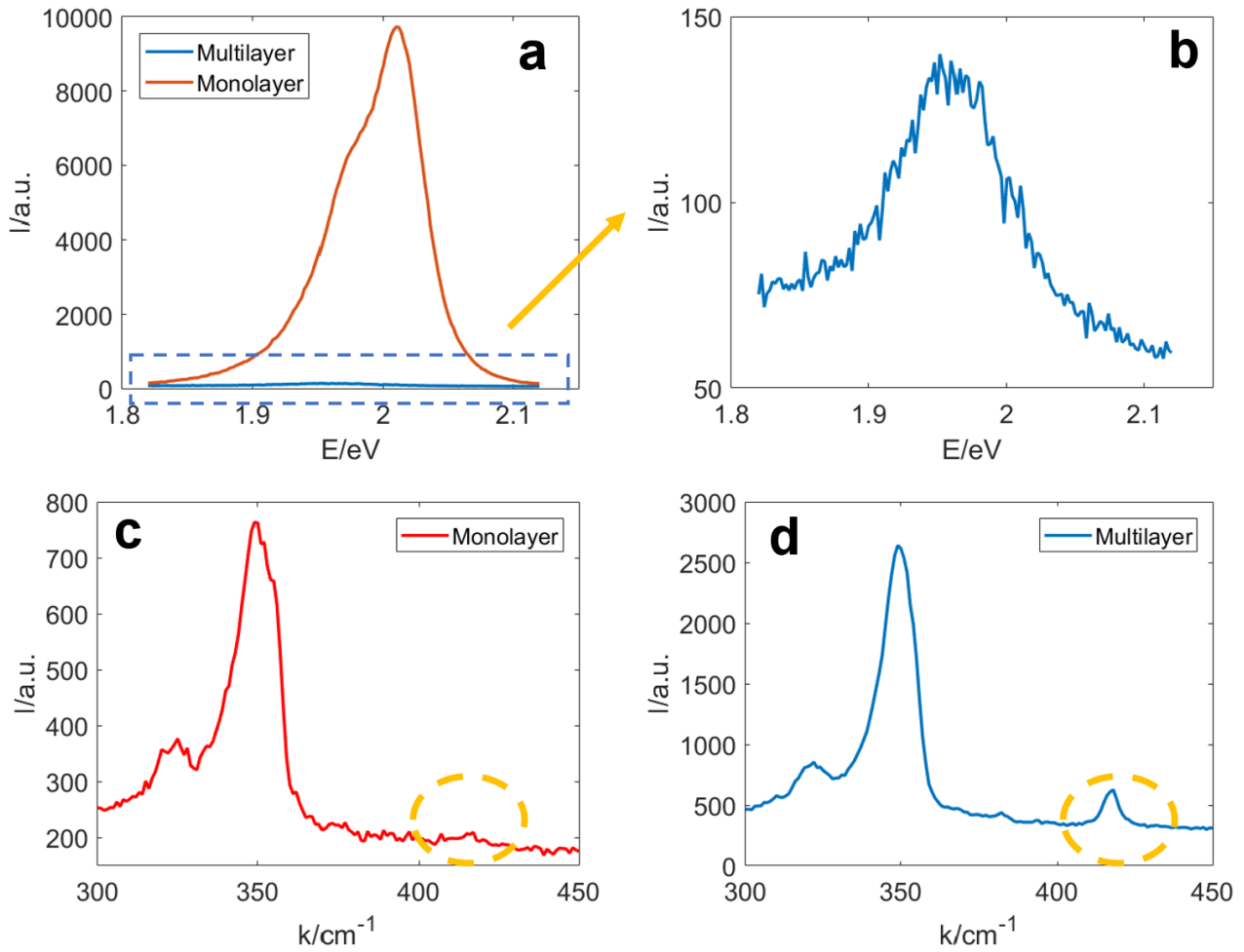


Figure S1. Distinguishing mono- and few-layer WS₂ by spectroscopy. (a) Photoluminescence (PL) spectroscopy of both a monolayer and a few-layer WS₂ crystal. (b) Magnified view of the suppressed PL for the few-layer sample. (c) Raman spectroscopy of monolayer WS₂. (d) Raman spectroscopy of few-layer WS₂.

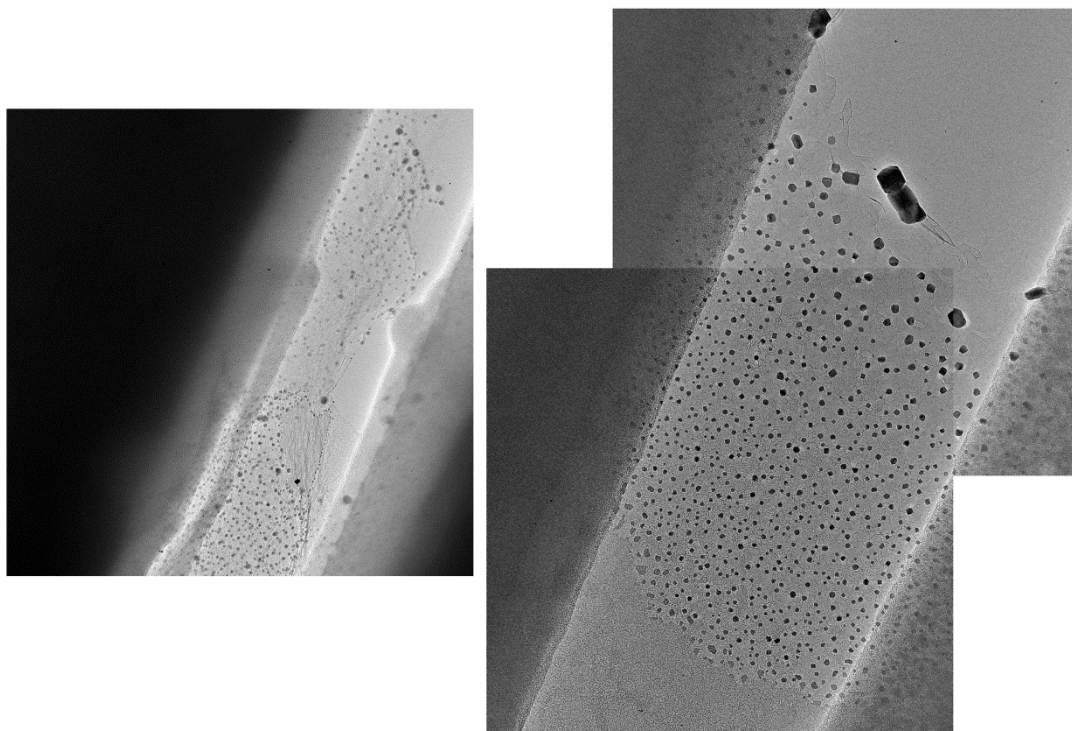


Figure S2. Low magnification TEM images of two separate monolayer WS₂ devices following the breakdown. The formed graphene was often irregular and twisted, and did not cover the entire area between the source-drain electrodes.

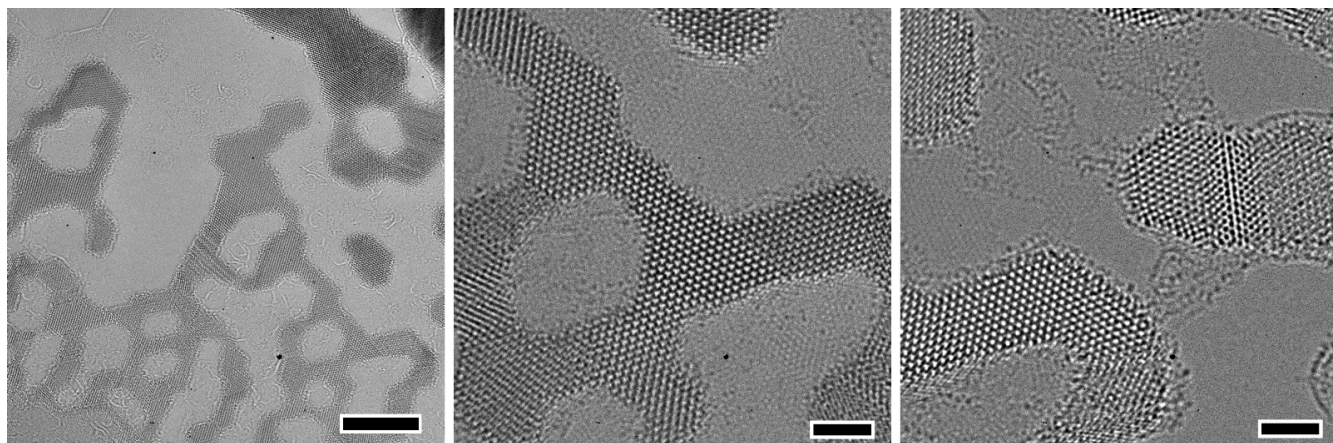


Figure S3. AC-TEM images of few-layer WS₂ after breakdown, showing faceting of the tendrils along the breakdown boundary. Scale bars 10 nm, 2 nm and 2 nm, respectively.

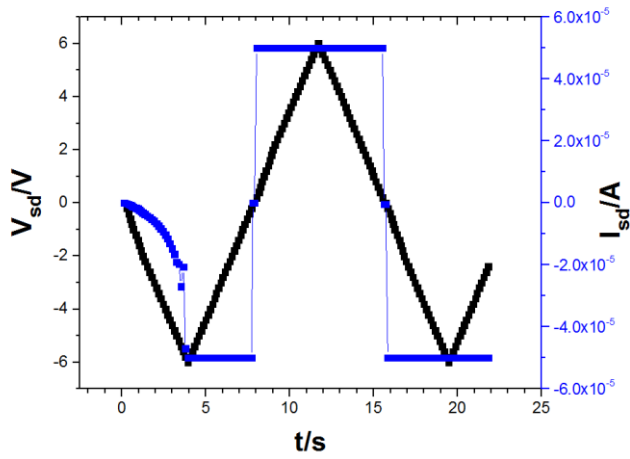


Figure S4. Potential cycling of a monolayer WS_2 . The first cycle results in irreversible hard breakdown, as seen on the second cycle.

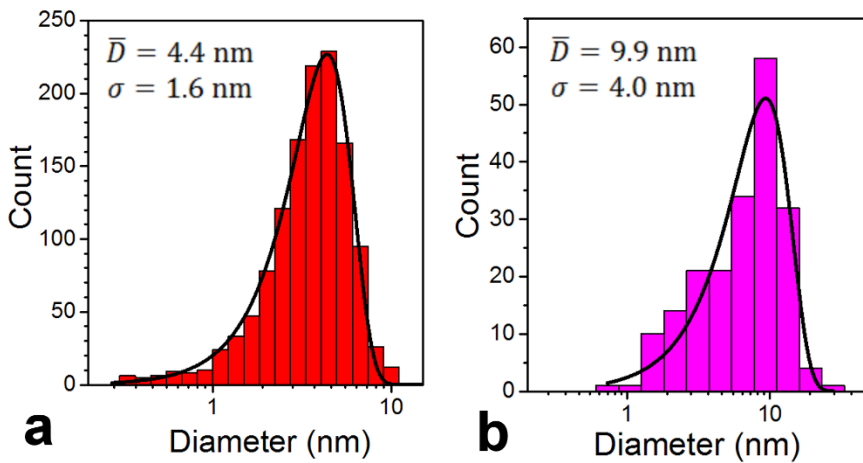


Figure S5. Size distributions for nanoparticles with Weibull fitting following breakdown of (a) monolayer, and (b) few-layer WS_2 .

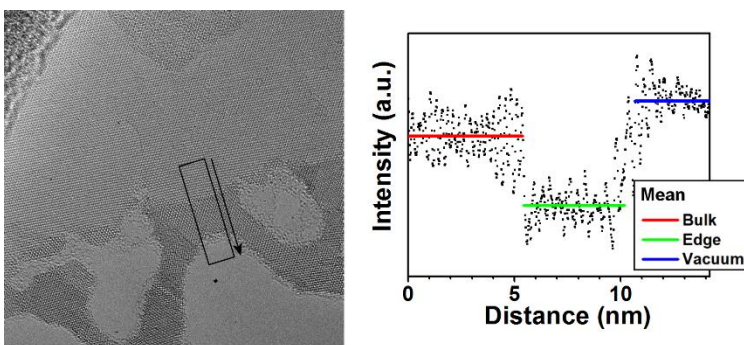


Figure S6. Wide-field view of a vaporization boundary and box-averaged intensity plot acquired from the rectangle along the indicated direction in the TEM image. Fit lines indicate the mean intensity values.

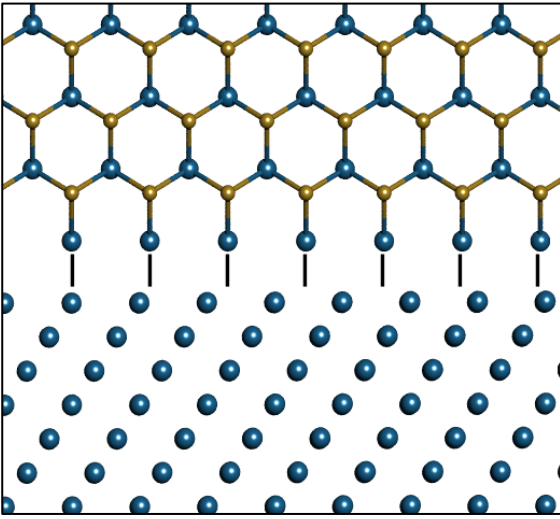


Figure S7. Atomic model sketch of pristine WS₂ and W (viewed down [110]) showing poor alignment along the interface.

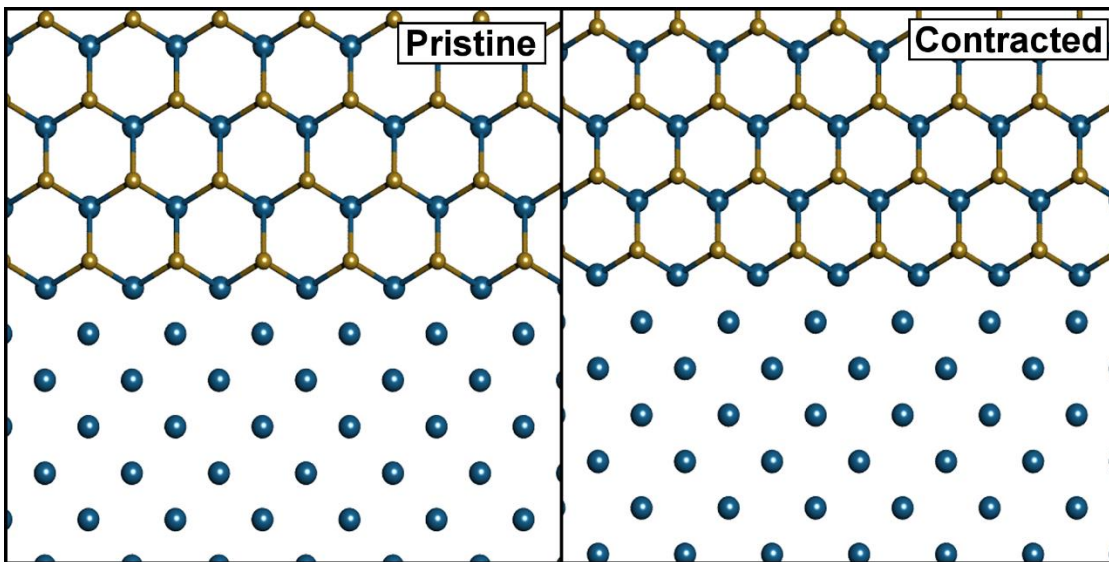


Figure S8. Atomic model sketches of WS₂ and W (viewed down [001]), showing good atomic alignment for pristine lattices, but poor alignment for WS₂ contracted lattice.

Current density model used in Figure 4

We solved the Poisson's equation as a simple model of the current density flowing between the two electrodes through the WS₂ channel. The Poisson's equation was solved using the Matlab Partial Differential Equation (PDE) toolbox. $-\nabla \cdot (\sigma \nabla V) = 0$ was solved in its 2D case, where σ is the conductivity, V is the voltage. $V = 0$ was set for the left square shaped electrode and $V = 1$ is set for the right square shaped electrode. The area of WS₂ was assumed to be much larger than the gap between electrodes to meet our experimental condition where either a large single domain or a continuous film is used. In practice, a PDE solving region 5 times larger than the width of electrodes

was taken. This size is large enough to give results in the area of interest. A natural Neumann boundary condition on the outer boundaries were used *i.e.* $\partial V/\partial n = 0$.